Journal of Integrative Neuroscience, Vol. 11, No. 3 (2012) 313–337

DOI: 10.1142/S0219635212500203

Imperial College Press
www.icpress.co.uk

EEG/fMRI fusion based on independent component analysis: Integration of data-driven and model-driven methods

Xu Lei[*,§], Pedro A. Valdes-Sosa[†] and Dezhong Yao[‡]

[*]*Key Laboratory of Cognition and Personality (Ministry of Education) and School of Psychology, Southwest University Chongqing, 400715, P. R. China*

[†]*Neuroimaging Department, Cuban Neuroscience Center Havana, 10600, Cuba*

[‡]*The Key Laboratory for NeuroInformation of Ministry of Education School of Life Science and Technology University of Electronic Science and Technology of China Chengdu, 610054, P. R. China*

[§]*xlei@swu.edu.cn*

[Received 17 June 2012; Accepted 6 August 2012; Published 18 September 2012]

Simultaneous electroencephalography (EEG) and functional magnetic resonance imaging (fMRI) provide complementary noninvasive information of brain activity, and EEG/fMRI fusion can achieve higher spatiotemporal resolution than each modality separately. This focuses on independent component analysis (ICA)-based EEG/fMRI fusion. In order to appreciate the issues, we first describe the potential and limitations of the developed fusion approaches: fMRI-constrained EEG imaging, EEG-informed fMRI analysis, and symmetric fusion. We then outline some newly developed hybrid fusion techniques using ICA and the combination of data-/model-driven methods, with special mention of the spatiotemporal EEG/fMRI fusion (STEFF). Finally, we discuss the current trend in methodological development and the existing limitations for extrapolating neural dynamics.

Keywords: EEG; fMRI; neuroimaging; fusion; ICA, Bayesian; STEFF.

1. Introduction

Electroencephalography (EEG) and functional magnetic resonance imaging (fMRI) are separate preeminent techniques in their ability for noninvasive mapping of brain process. Since the first study on data quality and patient safety (Ives *et al.*, 1993), the technology of simultaneous EEG/fMRI acquiring has matured (Laufs *et al.*, 2008). The EEG/fMRI fusion is a powerful approach not only to study the neuronal changes in cognitive neuroscience, but also to study endogenous brain oscillations during various mental states (Laufs *et al.*, 2008). There are excellent

[§]Corresponding author.

recent reviews of the theory and applications of EEG/fMRI (Debener *et al.*, 2006; Vulliemoz *et al.*, 2010a; Huster *et al.*, 2012). However, an area we felt deserved in-depth coverage was that of independent component analysis (ICA)-based EEG/fMRI fusion.

EEG and fMRI measure different attributes of brain activities. Scalp EEG potentials are generated by populations of cortical pyramidal neurons, with effective orientation perpendicular to the cortical surface (Niedermeyer & Da Silva, 2010). Postsynaptic potentials lasting longer than action potentials are believed to be the source of the EEG signals. Synchronous cortical activity over at least $6-10\,cm^2$ of gyral surface is necessary for events to be clearly detectable with scalp electrodes (Tao *et al.*, 2005). It is difficult to relate the measurements on the scalp to the underlying brain processes, partly due to the infolding and multi-laminar structure of the cortex (Megevand *et al.*, 2008). Some neuronal activity gives rise to a closed electric field (e.g., stellate cells), which is invisible to scalp electrodes (Nunez & Silberstein, 2000). Furthermore, due to volume conduction of the cerebrospinal fluid, skull and scalp, EEG data collected from any point on the scalp may include activity from multiple processes occurred within a large brain volume (Yao *et al.*, 2004). The transfer function from primary current to observed EEG, the lead field, imposes poor spatial resolution but is instantaneous. Thus, EEG has high temporal resolution for the underlying neuronal events.

fMRI measures blood oxygen level-dependent (BOLD) signal by detecting changes in magnetic susceptibility of oxy- and deoxy-hemoglobin. The interpretation of fMRI maps relies on the assumption that an increase of regional neuronal activity results in an increase in metabolic demand, an excessive increase in perfusion, and a decreased concentration of deoxygenated hemoglobin in local venous blood, and a subsequent increase of BOLD signal (Buzsaki *et al.*, 2007; Logothetis, 2008). The transformation from neuronal activity to BOLD signal, described by the hemodynamic response function (HRF), is low pass filter. Like all hemodynamic-based modalities, fMRI measures a surrogate signal reflecting neuronal mass activity whose temporal response is subject to both physical and biological constraints. Thus, BOLD signals unfold at a different time scale from the EEG (i.e., neuronal activity in ∼ms and BOLD in ∼s) (Glover, 1999). Spatially, fMRI studies typically use voxels with a volume of the order of $50\,mm^3$, and are well suited to the anatomic scale of the hemodynamic changes (Logothetis, 2008) and have relatively higher spatial resolution than EEG.

With EEG and fMRI combination, the features within mental process that need to be considered increased largely: neuroelectric, hemodynamic, endogenous, exogenous, stable, dynamic atc. An important challenge of EEG/fMRI fusion is to identify coupling and uncoupling between these features (Daunizeau *et al.*, 2010). Experimental work in monkeys showed that BOLD increases correlate better with increases in local field potential (LFP) than with multiunit activity (Logothetis *et al.*, 2001). LFP is linked to pyramidal neurons that generates scalp EEG potentials (Nunez, 1995). Thus, neurovascular coupling is obscure even during spontaneous brain

oscillations (Riera & Sumiyoshi, 2010). A recent study revealed that high- and low-frequency EEG oscillations independently contributed to explaining BOLD variance (Scheeringa *et al.*, 2011). In contrast, some other studies have shown uncoupling between modalities. The discordance may be associated with the distance between the neuronal population whose electrical activity is generating the EEG signal and the vascular tree, which provides the blood supply to these neurons (Beisteiner *et al.*, 1997). A number of physiological processes can cause hemodynamic BOLD changes without EEG correlates (Arthurs & Boniface, 2003). Such examples include neurotransmitter synthesis (Patel *et al.*, 2004), glial cell metabolism (Lauritzen, 2005), and the maintenance of steady-state transmembrane potential (Kida *et al.*, 2001). This differential sensitivity to neuronal activity can also arise when hemodynamic activity is caused by non-synchronized electrophysiological activity or if the latter has a closed source configuration that is invisible to EEG.

As the underlying mechanisms of EEG and fMRI do not wholly overlap, the methods of integration exhibit great diversity: spatial constraint versus temporal prediction, asymmetric versus symmetric fusion, and data- versus model-driven fusion (Trujillo-Barreto *et al.*, 2001; Daunizeau *et al.*, 2007; Valdes-Sosa *et al.*, 2009a). Independent component analysis does not require prior hypotheses about the connection of interest; hence, it is attractive for the exploration of the complementary advantage of EEG and fMRI. As a flexible framework is mandatory in data fusion, a systematic review on ICA-based approaches is helpful to understand the potential and limitations of the current methods. We begin with a classification of the different methods into a few categories and discuss them one by one. Then a new technique is introduced: the spatial-temporal EEG/fMRI fusion (STEFF). Finally, we discuss current trends in methodological development and identify the scientific questions in EEG/fMRI fusion.

2. EEG/fMRI Integration

There are currently three broad potential approaches to the EEG/fMRI integration (Eichele *et al.*, 2005; Daunizeau *et al.*, 2010; Laufs, 2012): (i) fMRI-constrained EEG imaging, where spatial information from fMRI signal is used for source reconstruction of the EEG signal (Liu *et al.*, 1998; Dale *et al.*, 2000; Lei *et al.*, 2011c, 2012); (ii) EEG-informed fMRI analysis, where the fMRI signal is modeled with features from EEG convolved with a HRF (Martinez-Montes *et al.*, 2004; Debener *et al.*, 2005; Eichele *et al.*, 2008b); and (iii) EEG/fMRI symmetric fusion, where a common generation model is constructed to explain both the EEG and fMRI data (Trujillo-Barreto *et al.*, 2001; Daunizeau *et al.*, 2007; Deco *et al.*, 2008; Valdes-Sosa *et al.*, 2009a).

2.1. *fMRI-constrained EEG imaging*

This technique uses spatial information from fMRI for source reconstruction of the EEG. First, the volume conductor for EEG imaging should be constructed; various models have been introduced in literature (Dale & Sereno, 1993; Henson *et al.*, 2009).

The simplest model is a sphere that yields analytical solutions (Yao, 2000) while others give a more accurate description of individual head and brain morphology (Dale & Sereno, 1993; Hagler *et al.*, 2009). Obtaining an accurate tessellation of the cortical surface via segmenting MRI is not a trivial problem. A practical implication is the employment of inverse-normalized canonical mesh (Ashburner & Friston, 2005). In this scheme, a cortical mesh is created from an MRI of a template brain and is transformed into a standard stereotactic space (Talairach & Tournoux, 1988). This template mesh is warped to match an individual's MRI using the inverse transformation of spatial normalization procedures (Ashburner & Friston, 2005). The generated canonical mesh provides a one-to-one mapping between the individual's source space and the template space, facilitating group analyses (Litvak & Friston, 2008) and incorporation of spatial priors (Henson *et al.*, 2010; Lei *et al.*, 2011c). The improved performances of the canonical mesh have been evaluated in simulation and real data tests (Mattout *et al.*, 2007; Henson *et al.*, 2009).

There are usually two models for source structure: equivalent current dipole and distributed source (Baillet *et al.*, 2001). The dipole is a convenient representation for coherent activation of a large number of pyramidal cells, possible extending over a few square centimeters of activated cortex. The equivalent current dipole model estimates the localization and orientation of one or a few equivalent dipoles generating a given scalp map as recorded by EEG electrodes. In contrast, distributed source model estimates the activity of each point in a solution space. This model is suited for extended sources but require further assumptions to relieve the ill-posed problem (Helmholtz, 1853; Yao, 1996). Both the equivalent dipole model and distributed source model have their own advantages. Recently, we proposed a Gaussian source model (GSM) to integrate them both (Lei *et al.*, 2009a). GSM is based on the parallel array of pyramidal neuron and the propagate property of cortical activity. The GSM can flexibly imitate the equivalent dipole and distributed source model by adopting extreme supporting range parameters of the Gaussian function. Sources with different spatial extension can be recovered through adaptive adjustments of the scale. Meanwhile, Friston *et al.* (2008) introduced an alternative inversion to automatically select either a sparse or distributed model depending on the data. Both models are integrations of previous extreme source models, and are physiologically reasonable for EEG source reconstruction. Notice there are vast source models based on multiple penalties; these models can also integrate the virtue of previous extreme source models (Valdes-Sosa *et al.*, 2009b; Wipf & Nagarajan, 2009).

Previous studies use fMRI activation to constrain the spatial locations of EEG source (Liu *et al.*, 1998; Dale *et al.*, 2000; Phillips *et al.*, 2002; Liu *et al.*, 2009) or initialize the dipole seeds (Stancak *et al.*, 2005; Auranen *et al.*, 2009). This has undesirable consequences when fMRI was considered the "truth" for spatial information (Dale *et al.*, 2000), since the relative importance of EEG and fMRI is not evaluated (Gonzalez Andino *et al.*, 2001). A Bayesian framework may relax the direct correspondence between modalities (Henson *et al.*, 2010). In the Bayesian framework, the posterior probability of a hypothesis is inferred from the probability of priors and

experimental observations (Lei *et al.*, 2009b; Quiros *et al.*, 2010). This provides us with the ability to probabilistically incorporate different spatial patterns from the fMRI. The final level of concordance between EEG and fMRI will be updated in the light of new, relevant data. This framework enabled us to develop a network-based source imaging (NESOI) system that employs multiple fMRI functional networks as a source location prior to where the intrinsic brain activity with correlated fluctuations is first introduced to constrain the spatial locations of EEG source (Lei *et al.*, 2011c, 2012).

2.2. *EEG-informed fMRI analysis*

EEG-informed fMRI analysis uses EEG as a predictor variable in the fMRI time-series model (Groening *et al.*, 2009; Vulliemoz *et al.*, 2010a). Based on the assumption of linear neurovascular coupling, previous studies convolved EEG features with a standard HRF (Lange & Zeger, 1997). In this fashion, the hemodynamic correlates of EEG rhythms (Goldman *et al.*, 2002; Laufs *et al.*, 2003a) and interictal EEG phenomena in epilepsy (Salek-Haddadi *et al.*, 2003) were first studied, followed by adaptive modulations of event-related responses (Debener *et al.*, 2006). However, several reports showed variability in the shape of the HRF as a function dependent on regions, subjects, age, task, sex, and sessions (Aguirre *et al.*, 1998; Miezin *et al.*, 2000; Gotman, 2008; LeVan *et al.*, 2010; Masterton *et al.*, 2010). To enhance the accuracy of EEG-informed fMRI analysis, we developed a scheme using classified EEG-defined events (Luo *et al.*, 2010). Various interictal epileptic discharges are grouped into different subclasses, and are separately used for foci localization. Thus, the imaging of the localizable foci can be enhanced largely even using the canonical HRF.

Considering the variability of the HRF context, a method that is independent of a specific shape of BOLD response may be an attractive alternative (Benar *et al.*, 2002; Gotman, 2008; Sturzbecher *et al.*, 2009; Sato *et al.*, 2010). However, the main obstacle for these approaches is the large number of parameters. Bayesian framework provides us with the ability to probabilistically incorporate the expected HRF shape, which is a good framework to integrate strengths in different HRF models. A robust Bayesian general linear model for HRF estimation has the advantage of not introducing bias into the estimation, since the smooth constraints imposed are soft priors and are clearly derived from physiological requirements (Marrelec & Benali, 2001; Lei *et al.*, 2010, 2011a).

The reliability of EEG-defined events is a noteworthy topic for resting state studies. The BOLD response is supposed to depend on a specific frequency content of neuronal activity, while others suggest that total power accounts for the changes in BOLD or the dynamics of the various frequency components, such as the relative magnitude of high and low frequencies (Rosa *et al.*, 2010). EEG rhythm studies have shown that the relationship between EEG and fMRI may be misled by high correlation between different frequency-band EEG signals (de Munck *et al.*, 2007). These problems can be remedied by multiple regressions of the BOLD signal on all EEG

frequency bands or decomposed features (Laufs *et al.*, 2003a; Mantini *et al.*, 2007; Eichele *et al.*, 2008a). Current choices of confounds include motion regressors and cardiac confounds (de Munck *et al.*, 2007). A conservative scheme is to include as many design confounds as possible to model other sources of variance in the BOLD signal (Scheeringa *et al.*, 2011). Furthermore, the EEG reference should be considered to set reliable EEG events, among which the reference electrode standardization technique (REST) is a novel appropriate choice (Yao, 2001; Qin *et al.*, 2010).

2.3. *EEG/fMRI symmetrical fusion*

EEG/fMRI symmetrical fusion refers to the use of a common forward or generative model that can explain both modalities. In contrast, the asymmetrical integrations in Secs. 2.1 and 2.2 give one modality privileged status as a priori information for the other modality (Trujillo-Barreto *et al.*, 2001). We can further categorize the symmetrical fusion to model- or data-driven fusion.

Model-driven symmetric fusion usually is predicated on the activity of an ensemble of postsynaptic potentials. This has two effects that translates into net primary current densities and then to EEG; and alternatively translates into vasomotor feed forward signal and then to BOLD. A review on model-driven fusion of brain oscillations can be found in Valdes-Sosa *et al.* (2009a). Dynamic causal models (DCM) is another framework for models of neuroelectric and metabolic activity in neuronal populations (Friston *et al.*, 2003; Kiebel *et al.*, 2007; Chen *et al.*, 2012). Neural field model provides another framework to integrate macroscopic models at large spatial scales with models at the microscopic scale (Chauvet, 1993; Poznanski & Riera, 2006). As model-driven fusions usually are neurophysiologically grounded, inversion of these models might provide us with the key insights into the genesis of neuronal activity and how it is mediated by intrinsic−extrinsic connections (Riera *et al.*, 2005; Valdes-Sosa *et al.*, 2009a; Coombes, 2010).

As the complexity of real metabolic−hemodynamic cascades renders the estimation of model-driven fusion problematic, some researchers have relied on measuring mutual dependence between EEG and fMRI signals, i.e., the symmetric fusion (Valdes-Sosa *et al.*, 2009a). Most work on data-driven fusion has mapped measures of association or covariation of the EEG and BOLD signal. In this approach, the BOLD signal is usually considered to have the same time evolution as the EEG. A multilinear version of partial least squares (Martinez-Montes *et al.*, 2004) carries out EEG/fMRI fusion by a combination of spatial, temporal and frequency signatures of the EEG. This method ensures maximal covariance of temporal signatures of EEG with those of BOLD. An even more comprehensive approach is that of Valdes-Sosa *et al.* (2009a) who gained fusion by measuring the correlation between estimated signals by solving the spatial inverse problem for the EEG and the temporal inverse problem for BOLD. These approaches are usually hampered by the lack of detailed information about neurovascular coupling. This was remedied by a common spatial

assumption in both modalities. In Daunizeau *et al.* (2007), the authors restricted common parameters to the position and extent of the EEG and fMRI sources.

Joint EEG/fMRI ICA decompositions provide a natural framework to integrate the two modalities (Eichele *et al.*, 2009). Several new methods based on ICA employ simplified neurovascular coupling models that integrate model- and data-driven fusions (Debener *et al.*, 2005; Goldman *et al.*, 2009; Luo *et al.*, 2010). We will discuss these methods in detail in Sec. 3.1.

As mentioned in Daunizeau *et al.* (2010), any symmetric fusion confronts two problems. First, the common substrate underlying EEG and fMRI signals should be identified by the fusion method. Second, when inferring this common subspace, the uncertainty should be decreased by the fusion method. The key strength of the data-driven fusion is its ability to provide empirical constraints for modeling (Valdes-Sosa *et al.*, 2009a). However, only model-driven fusion can provide us with a deeper understanding of neural mechanisms. Further improvements depend on the integration of model- and data-driven fusions.

3. Hybrid Fusion

EEG−fMRI coupling varies for different brain states and regions, and the proliferating number of fusion methods each reflects different ideas on how to model this phenomenon. Methodological and conceptual developments increasingly suggest that a flexible hybrid method based on the integration of data- and model-driven methods may be the best strategy for EEG/fMRI fusion. Such a method should have an adaptable framework that comprises both a generative model and a signal processing scheme simultaneously. Here we propose one possible candidate: the ICA-based fusion.

3.1. *The ICA-based fusion*

ICA was developed to decompose mixed signals and therefore seems ideal to address the convolution operators implicit in the forward problems of the EEG (spatial) and fMRI (temporal) signals. It is therefore unsurprising that ICA has become increasingly popular for analyzing brain imaging data (Makeig *et al.*, 1997; McKeown *et al.*, 1998; Chen & Yao, 2004). When considering the fusion problem, one must take into consideration the differences in spatial and temporal resolution of each modality. This suggests the following approach. For the EEG, source activations are assumed to be temporally independent of one another; therefore temporal ICA (tICA) is a reasonable choice, which is bolstered by the insufficient spatial sampling of this type of signal. For the fMRI, the sparsely distributed nature of the spatial pattern for typical cognitive activation paradigms seems compatible with the framework of spatial ICA (sICA). A strength of this choice is that prototypical EEG and image artifacts are also sparse and localized along the selected dimensions (McKeown *et al.*, 1998).

As illustrated in Fig. 1, the combinations of ICA and matching schemes engender various ICA-based EEG/fMRI fusions. Notice that this framework can be configured

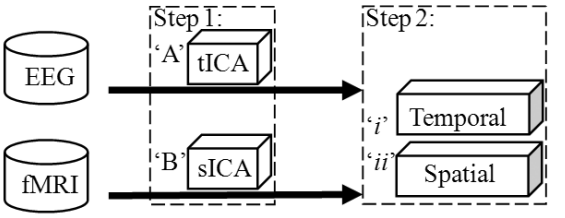

Step 1: Signal process, 'A' EEG temporal ICA; 'B' fMRI spatial ICA

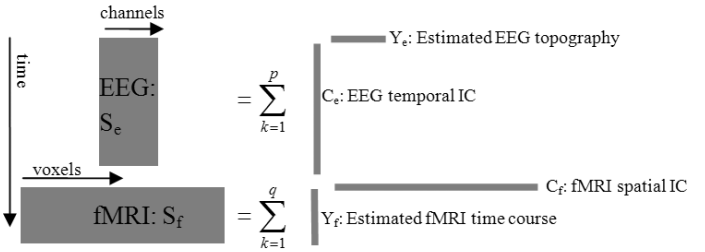

Step 2: Component matching, '*i*' temporal domain; '*ii*' spatial domain.

'*i*': Temporal domain		'*ii*': Spatial domain	
A-*i*	$C_e \leftrightarrow S_f$	A-*ii*	$Y_e \leftrightarrow S_f$
B-*i*	$S_e \leftrightarrow Y_f$	B-*ii*	$S_e \leftrightarrow C_f$
A/B-*i*	$C_e \leftrightarrow Y_f$	A/B-*ii*	$Y_e \leftrightarrow C_f$

$S_e \in R^{l\times n}$, $Y_e \in R^{1\times n}$, $C_e \in R^{l\times 1}$			
$S_f \in R^{u\times v}$, $C_f \in R^{1\times v}$, $Y_f \in R^{u\times 1}$			
n	~100	u	~100
l	~10K-100K	v	~10K-100K
p	~10	q	~10

Fig. 1. Various ICA-based EEG/fMRI fusions. Data flow from raw EEG and fMRI data to the correlation between modalities. Signal process: "A" is temporal ICA on EEG; "B" is spatial ICA on fMRI. Component matching: "*i*" is in temporal domain and "*ii*" is in spatial domain. The sizes and shapes of the matrices used by different fusion method are depicted heuristically.

to allow tensor ICA (Groves *et al.*, 2011) or multiway analysis (Martinez-Montes *et al.*, 2004). Raw EEG and fMRI data first undergo a modality-specific preprocessing; then, features are extracted by ICA and independent components (IC) from different modalities are matched in the spatial or temporal domain. Various ICA-based fusions can be chosen in a given context. Procedure "A-*i*": this is a popular EEG-informed fMRI fusion (Debener *et al.*, 2005; Goldman *et al.*, 2009). In this scheme, single-trial event-related potentials (ERPs) are decomposed in EEG to create the time course of events. These events are then convolved with a HRF, and used as a regressor in standard general linear model (GLM) analysis (Luo *et al.*,

2010). This procedure can be extended to "A-*i/ii*", which estimates source localizations problem using the EEG IC as the candidate time courses of EEG and BOLD signals (after convolving with a HRF (Brookings *et al.*, 2009)). If we employ ICA on fMRI signal and leave EEG unchanged, this will yield other fusion procedures: "B-*i*" and "B-*ii*". Procedure "B-*i*" uses the time course of fMRI component to match with the trial-by-trial variability of the ERPs. In Mantini *et al.* (2009), the authors found several fMRI brain functional networks account for EEG sustained and transient activity during target detection. In contrast, procedure "B-*ii*" uses the fMRI components directly as source location priors for EEG source imaging (Lei *et al.*, 2011c, 2012). This method, termed NESOI, can be considered a matching scheme in the spatial domain.

Decomposing the EEG and fMRI simultaneously (i.e., "A/B" in Fig. 1) engenders many other fusions. Procedure "A/B-*i*" can be realized in two ways. Moosmann *et al.* (2008) provided a single-trial joint ICA, which puts EEG and fMRI signal-trial data into a joint space. Signals need undergo typical preprocessing, including convolution or deconvolution to compensate for the hemodynamic lag. Another strategy, parallel group ICA (Eichele *et al.*, 2008a) involves two stages: first, recovering time courses from the group combined EEG and fMRI data using ICA in each modality, followed by matching components by correlating their trial-to-trial modulation. The last procedure "A/B", joint ICA (jICA), does not have any matching step. Instead of working with single trials, joint ICA (jICA) combines the average ERPs (frequently only at one channel) and fMRI contrast images for a group of subjects into a single ICA analysis. jICA derives a spatiotemporal solution with jointly estimated maximally independent sources of between-subject effects (Calhoun *et al.*, 2006). A shortcoming of the described procedures is that they do not explicitly state generative models. This problem is remedied with a procedure of type "A/B-*i/ii*" termed "Spatio-Tempral EEG/fMRI Fusion" (STEFF), which will be introduced in detail in Sec. 3.2.

We list the different ICA-based approaches in Table 1, where their properties, concise description, and related references are gathered. In this table, a great variety of schemes have been collated. Interestingly, there are some schemes that have not dealt with the EEG/fMRI fusion literature, such as procedures "A-*ii*", "B-*i/ii*" and "A/B-*ii*". Important virtues of the ICA-based fusion methods include the implicit removal of artifacts and noise, the ability to include prior information, and to allow group inferences. In the above, ICA provides a low-dimensional projection in which not only can EEG and fMRI common components (illustrated in cylinder III in Fig. 2) be analyzed explicitly, but the single modality sensitive components (illustrated in cylinders I and II in Fig. 2) also be visualized and analyzed explicitly. Moreover, using ICA, the computational load of fusion can be reduced greatly. Regional differences among brain scans are characterized by a handful of components instead of the original hundreds of thousands of voxels or hundreds of electrodes.

Table 1. The ICA-based EEG/fMRI fusion methods. Procedure is written in simplified form. For signal process, "A" is temporal ICA on EEG and "B" is spatial ICA on fMRI. For components matching, "*i*" is matching in temporal domain and "*ii*" in spatial domain.

Procedure	Name	Purpose of ICA	The Step-by-Step Instructions	Ref.
A-*i*	Single-trial EEG−fMRI	Extract trial dynamic	EEG-unmixing using ICA; the single trial EEG feature predicts the fMRI response	Debener *et al.*, 2005; Goldman *et al.*, 2009; Luo *et al.*, 2010
	Rhythm EEG−fMRI	Temporal hypotheses	Separate specific rhythm from EEG using ICA; EEG-informed fMRI	Scheeringa *et al.*, 2008
A-*i/ii*	Model-reduced joint inverse	Temporal hypotheses	Producing candidate EEG signals using ICA; convolving HRF to produce candidate BOLD signals; fitting simultaneously a solution to both modalities	Brookings *et al.*, 2009
B-*i*	Temporal correlation	Temporal hypotheses	Extracting temporal coherent networks from fMRI using ICA; matching EEG trial-by-trial variability (HRF convoluted) with the time-courses of fMRI components	Mantini *et al.*, 2009
B-*ii*	NESOI	Spatial priors	Extracting spatial prior from fMRI using ICA; fMRI-constrained ERP imaging	Lei *et al.*, 2011c; Lei *et al.*, 2012
A/B-*i*	Single-trial joint ICA	Fusion	Entering single-trial EEG and fMRI data into one joint space; the hemodynamic lag between trials is compensated by deconvolution; extraction linked components using ICA	Moosmann *et al.*, 2008
	Parallel group ICA	Temporal hypotheses	Recovering time courses from the group combined EEG and fMRI data using ICA in each modality; matching components by correlating their trial-to-trial modulation	Eichele *et al.*, 2008a
A/B	ERP/fMRI joint ICA	Fusion	Entering ERP waveform and fMRI activation map for each participant into one joint space; extraction linked components using ICA	Calhoun *et al.*, 2006
A/B-*i/ii*	STEFF	Specify temporal and spatial hypotheses	Adopting ICA to recover the time course and spatial mapping components from EEG and fMRI separately; linked components in the spatial and temporal domain using an Empirical Bayesian (EB) model	Lei *et al.*, 2010

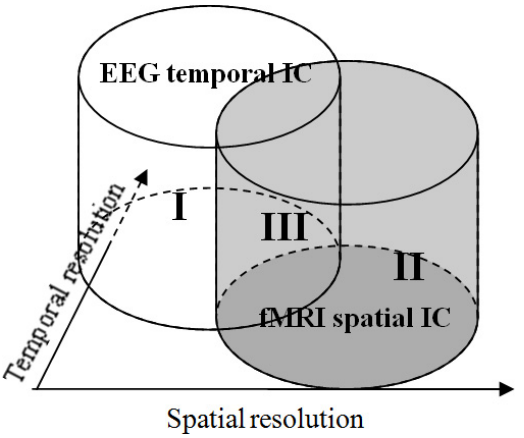

Fig. 2. The low-dimensional projection manifold for the ICA-based fusion. Using ICA, the signals are decomposed into two non-orthogonal subspaces: the white and gray cylinders contribute to the independent components of EEG and fMRI respectively. The intersection cylinder III defines the common substrate of neuronal activity. Conversely, the cylinder I (respectively II) denotes the subspace of neuronal activity detected by EEG (or fMRI) that does not contribute to fMRI (or EEG) measurements.

3.2. *Spatial–temporal EEG/fMRI fusion*

Spatial−temporal EEG/fMRI fusion (STEFF) employs spatial constraint and temporal prediction fusions in parallel in the unmixed space (Lei *et al.*, 2010). In Fig. 3, EEG and fMRI information is decomposed by data-driven methods into temporal and spatial compressed components. Their complementary features are apparent in each domain, and are fused between modalities using a model-driven method. STEFF can be described as being comprised of the following steps:

First, ICA decomposition on the original data. For a single subject, suppose tICA on EEG generates p tIC (waveforms) and the corresponding p topographies. Suppose sICA on fMRI generates q sIC (spatial patterns) and the corresponding time courses. This procedure can be replaced with group ICA in group inferences (Calhoun *et al.*, 2001), and group maps and time courses for both EEG and fMRI will be invoked (Lei *et al.*, 2010).

Second, EEG source imaging. The fMRI spatial IC patterns (the top center panel) are employed as the covariance priors (constraints) of the EEG source distribution to find the voxel-wise description of the electric responses (the top left panel) of the topography (the bottom left panel) of an EEG temporal IC. With q sIC of fMRI, each topography is projected to the cortex surface (p EEG tIC in total).

Third, hemodynamic response function estimation. The EEG time courses (the bottom center panel), which are the trial-by-trial dynamics extracted from EEG temporal IC (not shown here), are utilized to form the design matrix of the fMRI time course (the right panel) of each fMRI spatial IC to estimate (predict) the hemodynamic response function (the bottom right panel), and then to reconstruct its

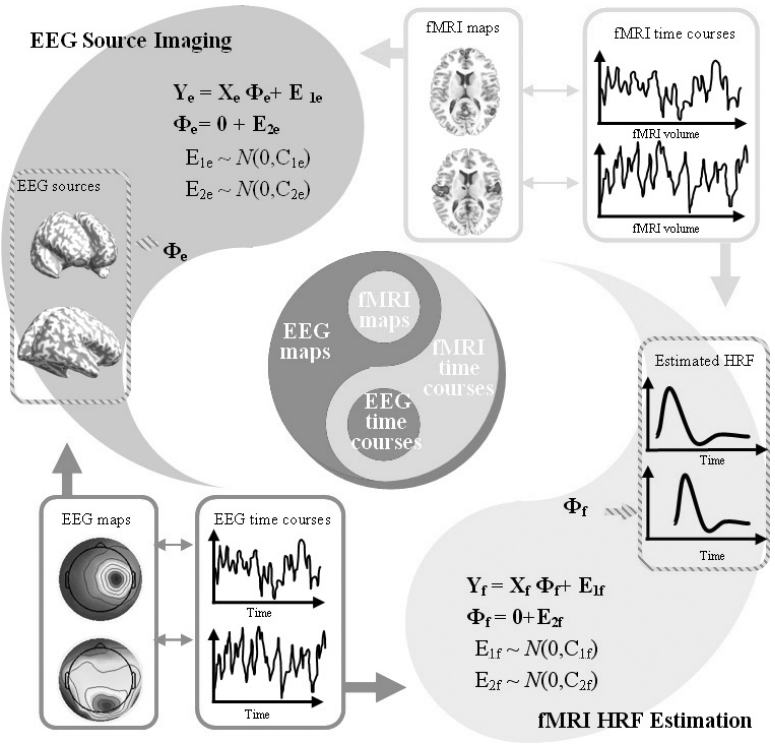

Fig. 3. STEFF employs constrain and prediction for information integration in parallel (adapted from Lei *et al.* (2010)). The fMRI spatial IC patterns (the top center panel) are employed as the covariance priors (constraints) of the EEG source distribution to find the voxel-wise description of the electric responses (the top left panel) of the topography (the bottom left panel) of an EEG temporal IC. The EEG time courses (the bottom center panel), which are the trial-by-trial dynamics extracted from EEG temporal IC (not show here), are utilized to form the design matrix of the fMRI time course (the top right panel) of each fMRI spatial IC to estimate (predict) the hemodynamic response function (the bottom right panel), and then to reconstruct its neuronal fluctuation. Further mathematical details are given in the Appendix.

neuronal fluctuation. With p tIC of EEG, each fMRI time course can reconstruct their HRF (q HRF in total).

The above steps constitute a parallel fusions in the temporal and spatial domains, and further mathematical details are given in Appendix (Lei *et al.*, 2011c).

A similar hierarchical linear model is employed in Fig. 3. For "EEG source imaging" (the left area in Fig. 3), to find the voxel-wise description of the topography of an EEG IC, fMRI IC patterns are employed as the covariance priors for EEG source distribution. Considering that some EEG sources may be blind for fMRI measurements, we employ multiple sparse priors (Friston *et al.*, 2008) for the remaining source space outside the subspace generated by fMRI IC. The balance between regions I and III in Fig. 2 is implemented by containing both fMRI IC and multiple sparse priors for spatial priors (Lei *et al.*, 2011c, 2012). This scheme differs from other fMRI-constrained EEG imaging methods (Dale *et al.*, 2000; Baillet *et al.*, 2001) where fMRI activation is adopted equivalently. In STEFF, the different spatial patterns are

given different weights by Empirical Bayesian (EB), thus the constraints can be flexible and realistic. For "fMRI HRF estimation" (the right area in Fig. 3), the trial-by-trial dynamics extracted from EEG IC acts as the prediction information and forms the design matrix for fMRI HRF estimation. The stimulus function, which encodes a generic obligatory response to target stimuli of constant amplitude, is also implemented to associate with exogenous features of the evoked response and other tasks. This scheme is used to maintain the balance between regions II and III in Fig. 2. The estimated HRF is region-specific and physiologically smoothed because of the adoption of a smoothness constraint.

The STEFF procedure is not only an integration of data- and model-driven methods, but also achieves a balance between the spatial and temporal domains. In examining the link between EEG and fMRI (see cylinder III in Fig. 2), EEG source imaging enables multiple fMRI spatial maps to match EEG topography, and fMRI HRF estimation enables multiple EEG trial amplitudes to match an fMRI time course. As a result, mappings are reconstructed as the common substrate of neuronal activity. Noticeably, the mappings are sparse and robust when facing mismatching situations in the spatial or temporal domain (Lei *et al.*, 2010).

3.3. *The data- versus model-driven fusion*

Generally, data-driven fusion is applied to data when specific hypotheses on spatial and temporal relationships are unavailable, or ill-specified, such as situations where traditional inference tests (Friston *et al.*, 1995) are not justifiable or are too insensitive due to conservative significance thresholds. ICA is intrinsically a multivariate approach and is particularly useful for data fusion of multiple tasks or data modalities (Calhoun *et al.*, 2009b). Excepting ICA-based fusion in Sec. 3.1, we also emphasize there are a large number of possible fusion methods that have not been implemented in EEG/fMRI fusion. For example, using combined group-discriminative techniques (Sui *et al.*, 2009), the authors found that coefficient-constrained−independent component analysis (CC−ICA) is sensitive and accurate in detecting group differences (e.g., controls versus patients). This framework is further improved using canonical correlation analysis (Sui *et al.*, 2010). Recently, another method named linked ICA (Groves *et al.*, 2010) uses a modular Bayesian framework for simultaneously modeling and discovering common features across multiple modalities. Linked ICA automatically determines the optimal weighting of each modality, and can also detect single-modality structured components when present. Apparently, these methods are possibilities for developing new EEG/fMRI fusion techniques.

Compared with data-driven fusions, model-driven fusion requires an explicit biophysical model that illustrates postsynaptic potentials to EEG on one hand, and BOLD signals on the other hand (Valdes-Sosa *et al.*, 2009a). Simultaneous EEG and fMRI recordings add problems to the model-driven fusions because of the involvement of two multivariate spaces and many necessary specifications. There is an increased degree of complexity in determining which channels would be sensitive to

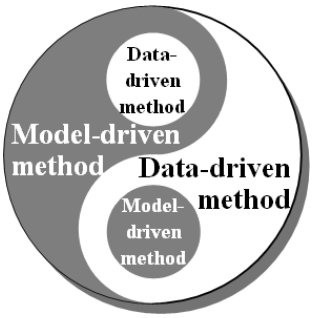

Fig. 4. Integration of data- and model-driven fusions. Despite the individuality between data and model, the integration and interaction of data and model might be promising for EEG/fMRI fusion.

event-related function, whose locations and latencies should be used to derive the event-related dynamics, whose regions in fMRI activation would be expected, and whose features should be utilized as fMRI predictors. However, only inversion of model-driven fusion can provide us with important insights into the nature and structure of cerebral activity (Friston *et al.*, 2003; Kiebel *et al.*, 2006).

Despite their individuality, the integration and interaction of data- and model-driven methods for EEG/fMRI fusion might be a promising approach to the EEG/fMRI fusion. As illustrated in Fig. 4, the data-driven method can provide empirical constraints for hierarchical relationships among different levels of cortices (Garrido *et al.*, 2007). In addition, the data-driven method provides a framework in which predictions from larger-scale computational models of electrophysiological and hemodynamic phenomena can be tested. For example, the approach may be used to locate the components that jointly reflect high-frequency EEG and low-frequency fMRI signals, respectively (Deco *et al.*, 2008).

4. Discussion

In this article, we systematically described ICA-based EEG/fMRI fusion. The complementary natures of simultaneous EEG/fMRI and the features of various integration methods are emphasized. As EEG and fMRI are volume-conducted and hemodynamics-convolved signal of brain activity, the correlations between modalities may be far from its neural mechanism. The ICA-based EEG/fMRI fusion is helpful in various experiments because of its flexible framework to integrate the data- and model-driven methods. With integration of neuroimaging techniques and cognitive computation, ICA-based EEG/fMRI fusion can adapt to different levels of concordance between EEG and fMRI. Future development of the EEG/fMRI fusion may help us analyze brain activity during natural stimulation (Hasson *et al.*, 2010) in situations closer to everyday-life such as watching movies, (Hasson *et al.*, 2004), driving (Calhoun & Pearlson, 2012), sleeping (Horovitz *et al.*, 2009), and decision making (Sajda *et al.*, 2009).

Below we discuss current trends in the methodological development of this fast-developing field.

4.1. *Fusion for large-scale brain network*

The next phase of cognitive neuroscience is to go beyond studying local brain regions and to begin learning about the global, distributed networks underlying cognitive activity. The dynamic information, regardless modeled within dynamic continuity (Cacha & Poznanski, 2011) or dynamic connectivity (Bullmore & Sporns, 2009), might allow defining precisely the timing and location of cognitive processes. For example, noninvasive dynamic imaging of epileptic brain can enhance our understanding of seizure generation and propagation (Tyvaert *et al.*, 2009). Future developments of the EEG/fMRI fusion require deeper understanding of the dynamics within and between distributed networks in the brain.

In order to reconstruct the large-scale neuronal dynamics, measurements with both high temporal and spatial resolution are essential. For fMRI, the temporal dynamics of IC (after ICA decomposition) has been utilized to examine the causality among different brain networks (Jafri *et al.*, 2008; Demirci *et al.*, 2009). Functional network connectivity (FNC) emerges as a powerful way to characterize the relationships between distributed brain networks, as opposed to functional connectivity which focuses upon the relationships between single voxels (Stevens *et al.*, 2009). Initial studies used the lag between time courses to examine FNC differences between schizophrenic and healthy controls (Jafri *et al.*, 2008). A recent improvement using Granger causality analysis (GCA) studies the direct interactions among networks (Demirci *et al.*, 2009; Porcaro *et al.*, 2009).

Identifying network interaction from the complementary neuroelectric and hemodynamic signals may help explain the complex relationships between different brain regions. A straightforward extension of fMRI FNC covers the interaction between EEG condensed components. The low spatial resolution of EEG can be improved by source localization techniques (Lei *et al.*, 2011c, 2012). The interactions between functional networks in each modality can be determined by GCA. Based on the NESOI-estimated matching between EEG and fMRI components, multimodal functional network connectivity (mFNC) provides a fusion for large-scale brain network (Lei *et al.*, 2011b). It may help explain the complex relationships between distributed cerebral sites in the brain and possibly provide new understanding of neurological and psychiatric disorders (Calhoun *et al.*, 2009a; Lei *et al.*, 2011b).

4.2. *Scientific questions in the EEG/fMRI fusion*

For some scientific investigations, fMRI is sufficient for questions of where and EEG is sufficient for questions of when (Friston, 2009). So what is the sort of scientific question that really requires EEG/fMRI fusion? This question is particularly important for functional neuroimaging. Initially, researchers used simultaneous EEG and fMRI to uncover the regions of the brain showing changes in the BOLD signal in response to epileptic spikes seen in the EEG. Established diagnostic application improves our understanding of the spatiotemporal mapping of epileptic networks (Groening *et al.*, 2009; Vulliemoz *et al.*, 2010b). Another promising application is

the study of rest-state network. Research in EEG (Laufs *et al.*, 2003b; Chen *et al.*, 2008) and fMRI (Damoiseaux *et al.*, 2006; Mantini *et al.*, 2007) have shown that these networks are pervasive in the resting state and during task performance, and hence provide robust measures of the interacted and disturbed brain activity. Recent work shows that the information contained within EEG microstates on a millisecond timescale is able to elicit BOLD activation patterns consistent with well-known rest-state networks (Britz *et al.*, 2010; Musso *et al.*, 2010; Van De Ville *et al.*, 2010).

Acknowledgment

The manuscript was substantially improved thanks to the thoughtful comments of the anonymous reviewer to whom we wish to extend our thanks. This project was funded by grants from the 973 project 2011CB707803, the National Nature Science Foundation of China (31070881, 31170953, 81071222, 31200857) and the 111 Project for neuroinformation of the Ministry of Education of China, the Fundamental Research Funds for the Central Universities (SWU1209319), National Key Discipline of Basic Psychology at Southwest University (NSKD11047) and Humanity and Social Science Youth foundation of Ministry of Education of China (12YJC190015).

Appendix

STEFF contains parallel fusions in the temporal and spatial domains (Lei *et al.*, 2010). Both are modeled with an EB model (Phillips *et al.*, 2005; Friston *et al.*, 2006):

$$\begin{cases} Y = X\Phi + E_1 & E_1 \sim N(0, C_1) \\ \Phi = 0 + E_2 & E_2 \sim N(0, C_2) \end{cases}, \tag{A.1}$$

For "EEG source imaging", $Y = Y_e^T \in R^{n\times 1}$ is one of the p-independent components EEG topographies with n channels. $X \in R^{n\times d}$ is the known lead-field matrix calculated for the selected head model, and $\Phi \in R^{d\times 1}$ is the unknown distribution of d dipoles. $N(0, C)$ denotes a multivariate zero-mean Gaussian distribution with covariance C. The terms E_1 and E_2 represent random fluctuations in channel and source spaces, respectively. These spatial covariances E_1 and E_2 are mixtures of covariance components at the corresponding levels. At the electrode space level, we assume $C_1 = \alpha^{-1} I_n$ to encode the covariance of electrode noise, where I_n is an $n \times n$ identity matrix. At the source space level, we express C_2 as the covariance components,

$$C_2 = \sum_{i=1}^{k} \lambda_i V_i, \tag{A.2}$$

where $\gamma \equiv [\lambda_1, \lambda_2, \ldots, \lambda_k]^T$ is a vector of k non-negative hyperparameters that control the relative contribution of each covariance basis matrix, V_i. The Green function, $G = 2\exp(A)$, models anatomic coherent sources and is a function of an adjacency matrix, A, with $A_{ij} \in [0, 1]$ encoding the neighboring relationships among nodes of the cortical mesh defining the solution space (Harrison *et al.*,

2007). The jth column of the Green function matrix G is q_j, encoding neighboring patches weighted by their surface proximity. Two different kinds of covariance matrices are employed:

$$\{V_i\} = \{V_i^f\} \cup \{V_i^e\}, \tag{A.3}$$

where V_i^e encodes multiple sparse priors (Friston *et al.*, 2008) that are sparsely sampled from a subspace of EEG source space that does not necessarily contribute to fMRI measurements and V_i^f encodes the prior coherence pattern information derived from fMRI. Each fMRI sIC is scaled to z scores and is mapped to construct V_i^f (Lei *et al.*, 2011c).

For "fMRI HRF estimation", Eq. (A.1) has very different explanations. In Eq. (A.1), $Y = Y_f \in R^{u\times 1}$ is one time course of the q fMRI sICs with u volumes (or time points), and $\Phi \in R^{d\times 1}$ is the unknown HRF for each time course ($d = lm$, l: order of the convolution model; m: number of stimulus functions). The covariance of E_1 is $C_1 = \alpha^{-1} I_u$ and C_2 is the discrete second order differentiation matrix that gives smooth constraints for HRF (Marrelec & Benali, 2001). $X \in R^{u\times d}$ is the design matrix, consisting of the lagged stimulus function matrix X_s. Given that $[x_1, x_2, \ldots, x_u]^T$, the ηth column of X_s, is an event time course, then X is

$$X = \begin{bmatrix} \cdots & x_1 & 0 & 0 & 0 & \cdots \\ \cdots & x_2 & x_1 & 0 & 0 & \cdots \\ \cdots & \vdots & \vdots & \ddots & 0 & \cdots \\ \cdots & x_l & x_{l-1} & \cdots & x_1 & \cdots \\ \cdots & \vdots & \vdots & \vdots & \vdots & \cdots \\ \cdots & x_u & x_{u-1} & \cdots & x_{u-l+1} & \cdots \end{bmatrix}, \tag{A.4}$$

i.e., the $(\eta-1)l+1$th to the ηlth columns of X contain the lagged ηth column of X_s. X_s consists of two kinds of stimulus functions:

$$X_s = [X_s^f X_s^e]. \tag{A.5}$$

The first stimulus function X_s^f encodes invariant evoked responses to target stimuli; the additional functions X_s^e encodes the "single trial quantification" of the EEG tIC, where the single trial quantifications are first decorrelated using Schmidt-Gram orthogonalization from the nonspecific hemodynamic response to stimulus onsets, ensuring the specificity of inferences from the electrophysiological predictors.

REFERENCES

Aguirre, G.K., Zarahn, E. & D'Esposito, M. (1998) The variability of human, BOLD hemodynamic responses. *Neuroimage*, **8**, 360–369.

Arthurs, O.J. & Boniface, S.J. (2003) What aspect of the fMRI BOLD signal best reflects the underlying electrophysiology in human somatosensory cortex? *Clin. Neurophysiol.*, **114**, 1203−1209.

Ashburner, J. & Friston, K.J. (2005) Unified segmentation. *Neuroimage*, **26**, 839−851.

Auranen, T., Nummenmaa, A., Vanni, S., Vehtari, A., Hamalainen, M.S., Lampinen, J. & Jaaskelainen, I.P. (2009) Automatic fMRI-guided MEG multidipole localization for visual responses. *Hum. Brain. Mapp.*, **30**, 1087−1099.

Baillet, S., Mosher, J. & Leahy, R. (2001) Electromagnetic brain mapping. *IEEE Signal Processing Magazine*, **18**, 14−30.

Beisteiner, R., Erdler, M., Teichtmeister, C., Diemling, M., Moser, E., Edward, V. & Deecke, L. (1997) Magnetoencephalography may help to improve functional MRI brain mapping. *Eur. J. Neurosci.*, **9**, 1072−1077.

Benar, C.G., Gross, D.W., Wang, Y., Petre, V., Pike, B., Dubeau, F. & Gotman, J. (2002) The BOLD response to interictal epileptiform discharges. *Neuroimage*, **17**, 1182−1192.

Britz, J., Van De Ville, D. & Michel, C.M. (2010) BOLD correlates of EEG topography reveal rapid resting-state network dynamics. *Neuroimage*, **52**, 1162−1170.

Brookings, T., Ortigue, S., Grafton, S. & Carlson, J. (2009) Using ICA and realistic BOLD models to obtain joint EEG/fMRI solutions to the problem of source localization. *Neuroimage*, **44**, 411−420.

Bullmore, E. & Sporns, O. (2009) Complex brain networks: Graph theoretical analysis of structural and functional systems. *Nat. Rev. Neurosci.*, **10**, 186−198.

Buzsaki, G., Kaila, K. & Raichle, M. (2007) Inhibition and brain work. *Neuron*, **56**, 771−783.

Cacha, L. & Poznanski, R. (2011) Associable representations as field of influence for dynamic cognitive processes. *J. Integr. Neurosci.*, **10**, 423−437.

Calhoun, V.D., Adali, T., Pearlson, G.D. & Kiehl, K.A. (2006) Neuronal chronometry of target detection: Fusion of hemodynamic and event-related potential data. *Neuroimage*, **30**, 544−553.

Calhoun, V.D., Adali, T., Pearlson, G.D. & Pekar, J.J. (2001) A method for making group inferences from functional MRI data using independent component analysis. *Hum. Brain Mapp.*, **14**, 140−151.

Calhoun, V.D., Eichele, T. & Pearlson, G. (2009a) Functional brain networks in schizophrenia: A review. *Front Hum. Neurosci.*, **3**, 17.

Calhoun, V.D., Liu, J. & Adali, T. (2009b) A review of group ICA for fMRI data and ICA for joint inference of imaging, genetic, and ERP data. *Neuroimage*, **45**, S163−S172.

Calhoun, V.D. & Pearlson, G.D. (2012) A selective review of simulated driving studies: Combining naturalistic and hybrid paradigms, analysis approaches, and future directions. *Neuroimage*, **59**, 25−35.

Chauvet, G. (1993) An n-level field theory of biological neural networks. *J. Math. Biol.*, **31**, 771−795.

Chen, A.C., Feng, W., Zhao, H., Yin, Y. & Wang, P. (2008) EEG default mode network in the human brain: Spectral regional field powers. *Neuroimage*, **41**, 561−574.

Chen, C.C., Kiebel, S.J., Kilner, J.M., Ward, N.S., Stephan, K.E., Wang, W.J. & Friston, K.J. (2012) A dynamic causal model for evoked and induced responses. *Neuroimage*, **59**, 340−348.

Chen, H. & Yao, D. (2004) Discussion on the choice of separated components in fMRI data analysis by spatial independent component analysis. *Magn. Reson. Imaging*, **22**, 827−833.

Coombes, S. (2010) Large-scale neural dynamics: Simple and complex. *Neuroimage*, **52**, 731−739.

Dale, A.M., Liu, A.K., Fischl, B.R., Buckner, R.L., Belliveau, J.W., Lewine, J.D. & Halgren, E. (2000) Dynamic statistical parametric mapping: Combining fMRI and MEG for high-resolution imaging of cortical activity. *Neuron*, **26**, 55−67.

Dale, A.M. & Sereno, M.I. (1993) Improved localizadon of cortical activity by combining EEG and MEG with MRI cortical surface reconstruction: A linear approach. *J. Cognitive Neurosci.*, **5**, 162−176.

Damoiseaux, J.S., Rombouts, S.A., Barkhof, F., Scheltens, P., Stam, C.J., Smith, S.M. & Beckmann, C.F. (2006) Consistent resting-state networks across healthy subjects. *Proc. Natl. Acad. Sci. USA*, **103**, 13848−13853.

Daunizeau, J., Grova, C., Marrelec, G., Mattout, J., Jbabdi, S., Pelegrini-Issac, M., Lina, J.M. & Benali, H. (2007) Symmetrical event-related EEG/fMRI information fusion in a variational Bayesian framework. *Neuroimage*, **36**, 69−87.

Daunizeau, J., Laufs, H. & Friston, K. (2010) EEG−fMRI information fusion: Biophysics and data analysis. *EEG-fMRI*, 511−526.

de Munck, J.C., Goncalves, S.I., Huijboom, L., Kuijer, J.P., Pouwels, P.J., Heethaar, R.M. & Lopes da Silva, F.H. (2007) The hemodynamic response of the alpha rhythm: An EEG/fMRI study. *Neuroimage*, **35**, 1142−1151.

Debener, S., Ullsperger, M., Siegel, M. & Engel, A.K. (2006) Single-trial EEG-fMRI reveals the dynamics of cognitive function. *Trends Cogn. Sci.*, **10**, 558−563.

Debener, S., Ullsperger, M., Siegel, M., Fiehler, K., von Cramon, D.Y. & Engel, A.K. (2005) Trial-by-trial coupling of concurrent electroencephalogram and functional magnetic resonance imaging identifies the dynamics of performance monitoring. *J. Neurosci.*, **25**, 11730−11737.

Deco, G., Jirsa, V.K., Robinson, P.A., Breakspear, M. & Friston, K. (2008) The dynamic brain: From spiking neurons to neural masses and cortical fields. *PloS. Comput. Biol.*, **4**, e1000092.

Demirci, O., Stevens, M.C., Andreasen, N.C., Michael, A., Liu, J., White, T., Pearlson, G.D., Clark, V.P. & Calhoun, V.D. (2009) Investigation of relationships between fMRI brain networks in the spectral domain using ICA and Granger causality reveals distinct differences between schizophrenia patients and healthy controls. *Neuroimage*, **46**, 419−431.

Eichele, T., Calhoun, V.D. & Debener, S. (2009) Mining EEG-fMRI using independent component analysis. *Int. J. Psychophysiol.*, **73**, 53−61.

Eichele, T., Calhoun, V.D., Moosmann, M., Specht, K., Jongsma, M.L., Quiroga, R.Q., Nordby, H. & Hugdahl, K. (2008a) Unmixing concurrent EEG-fMRI with parallel independent component analysis. *Int. J. Psychophysiol.*, **67**, 222−234.

Eichele, T., Debener, S., Calhoun, V.D., Specht, K., Engel, A.K., Hugdahl, K., von Cramon, D.Y. & Ullsperger, M. (2008b) Prediction of human errors by maladaptive changes in event-related brain networks. *Proc. Natl. Acad. Sci. USA*, **105**, 6173−6178.

Eichele, T., Specht, K., Moosmann, M., Jongsma, M.L., Quiroga, R.Q., Nordby, H. & Hugdahl K. (2005) Assessing the spatiotemporal evolution of neuronal activation with

single-trial event-related potentials and functional MRI. *Proc. Natl. Acad. Sci. USA*, **102**, 17798−17803.

Friston, K., Harrison, L., Daunizeau, J., Kiebel, S., Phillips, C., Trujillo-Barreto N., Henson, R., Flandin, G. & Mattout, J. (2008) Multiple sparse priors for the M/EEG inverse problem. *Neuroimage*, **39**, 1104−1120.

Friston, K., Henson, R., Phillips, C. & Mattout, J. (2006) Bayesian estimation of evoked and induced responses. *Hum. Brain. Mapp.*, **27**, 722−735.

Friston, K.J. (2009) Modalities, modes, and models in functional neuroimaging. *Science*, **326**, 399−403.

Friston, K.J., Harrison, L. & Penny, W. (2003) Dynamic causal modelling. *Neuroimage*, **19**, 1273−1302.

Friston, K.J., Holmes, A.P., Worsley, K.J., Poline, J.-P., Frith, C.D. & Frackowiak, R.S.J. (1995) Statistical parametric maps in functional imaging: A general linear approach. *Hum. Brain Mapp.*, **2**, 189−210.

Garrido, M.I., Kilner, J.M., Kiebel, S.J. & Friston, K.J. (2007) Evoked brain responses are generated by feedback loops. *Proc. Natl. Acad. Sci. USA*, **104**, 20961−20966.

Glover, G.H. (1999) Deconvolution of impulse response in event-related BOLD fMRI. *Neuroimage*, **9**, 416−429.

Goldman, R.I., Stern, J.M., Engel, J., Jr. & Cohen, M.S. (2002) Simultaneous EEG and fMRI of the alpha rhythm. *Neuroreport*, **13**, 2487−2492.

Goldman, R.I., Wei, C.Y., Philiastides, M.G., Gerson, A.D., Friedman, D., Brown, T.R. & Sajda, P. (2009) Single-trial discrimination for integrating simultaneous EEG and fMRI: Identifying cortical areas contributing to trial-to-trial variability in the auditory oddball task. *Neuroimage*, **47**, 136−147.

Gonzalez Andino, S., Blanke, O., Lantz, G., Thut, G. & Grave de Peralta Menendez, R. (2001) The use of functional constraints for the neuroelectromagnetic inverse problem: Alternatives and caveats. *Int. J. Bioelectromag.*, **3**.

Gotman, J. (2008) Epileptic networks studied with EEG-fMRI. *Epilepsia 49 Suppl.*, **3**, 42−51.

Groening, K., Brodbeck, V., Moeller, F., Wolff, S., van Baalen, A., Michel, C.M., Jansen O., Boor, R., Wiegand, G., Stephani, U. & Siniatchkin, M. (2009) Combination of EEG-fMRI and EEG source analysis improves interpretation of spike-associated activation networks in paediatric pharmacoresistant focal epilepsies. *Neuroimage*, **46**, 827−833.

Groves, A.R., Beckmann, C.F., Smith, S.M. & Woolrich, M.W. (2011) Linked independent component analysis for multimodal data fusion. *Neuroimage*, **54**, 2198−2217.

Hagler, D.J., Jr., Halgren, E., Martinez, A., Huang, M., Hillyard, S.A. & Dale, A.M. (2009) Source estimates for MEG/EEG visual evoked responses constrained by multiple, retinotopically-mapped stimulus locations. *Hum. Brain Mapp.*, **30**, 1290−1309.

Harrison, L.M., Penny, W., Ashburner, J., Trujillo-Barreto, N. & Friston, K.J. (2007) Diffusion-based spatial priors for imaging. *Neuroimage*, **38**, 677−695.

Hasson, U., Malach, R. & Heeger, D.J. (2010) Reliability of cortical activity during natural stimulation. *Trends Cogn. Sci.*, **14**, 40−48.

Hasson, U., Nir, Y., Levy, I., Fuhrmann, G. & Malach, R. (2004) Intersubject synchronization of cortical activity during natural vision. *Science*, **303**, 1634−1640.

Helmholtz, H. (1853) Ueber einige Gesetze der Vertheilung elektrischer Ströme in körperlichen Leitern mit Anwendung auf die thierisch-elektrischen Versuche. *Annalen der Physik und Chemie*, **165**, 211−233.

Henson, R.N., Flandin, G., Friston, K.J. & Mattout, J. (2010) A Parametric Empirical Bayesian framework for fMRI-constrained MEG/EEG source reconstruction. *Hum. Brain Mapp.*, **31**, 1512−1531.

Henson, R.N., Mattout, J., Phillips, C. & Friston, K.J. (2009) Selecting forward models for MEG source-reconstruction using model-evidence. *Neuroimage*, **46**, 168−176.

Horovitz, S.G., Braun, A.R., Carr, W.S., Picchioni, D., Balkin, T.J., Fukunaga, M. & Duyn, J.H. (2009) Decoupling of the brain's default mode network during deep sleep. *Proc. Natl. Acad. Sci. USA*, **106**, 11376−11381.

Huster, R.J., Debener, S., Eichele, T. & Herrmann, C.S. (2012) Methods for simultaneous EEG-fMRI: An introductory review. *J. Neurosci.*, **32**, 6053−6060.

Ives, J.R., Warach, S., Schmitt, F., Edelman, R.R. & Schomer, D.L. (1993) Monitoring the patient's EEG during echo planar MRI. *Electroencephalogr. Clin. Neurophysiol.*, **87**, 417−420.

Jafri, M.J., Pearlson, G.D., Stevens, M. & Calhoun, V.D. (2008) A method for functional network connectivity among spatially independent resting-state components in schizophrenia. *Neuroimage*, **39**, 1666−1681.

Kida, I., Hyder, F. & Behar, K.L. (2001) Inhibition of voltage-dependent sodium channels suppresses the functional magnetic resonance imaging response to forepaw somatosensory activation in the rodent. *J. Cereb. Blood Flow Metab.*, **21**, 585−591.

Kiebel, S.J., David, O. & Friston, K.J. (2006) Dynamic causal modelling of evoked responses in EEG/MEG with lead field parameterization. *Neuroimage*, **30**, 1273−1284.

Kiebel, S.J., Garrido, M.I. & Friston, K.J. (2007) Dynamic causal modelling of evoked responses: The role of intrinsic connections. *Neuroimage*, **36**, 332−345.

Lange, N. & Zeger, S.L. (1997) Non-linear Fourier time series analysis for human brain mapping by functional magnetic resonance imaging. *J. Royal Statistical Society: Series C* (*Applied Statistics*), **46**, 1−29.

Laufs, H. (2012) A personalized history of EEG-fMRI integration. *Neuroimage*, **62**, 1056−1067.

Laufs, H., Daunizeau, J., Carmichael, D.W. & Kleinschmidt, A. (2008) Recent advances in recording electrophysiological data simultaneously with magnetic resonance imaging. *Neuroimage*, **40**, 515−528.

Laufs, H., Kleinschmidt, A., Beyerle, A., Eger, E., Salek-Haddadi, A., Preibisch, C. & Krakow, K. (2003a) EEG-correlated fMRI of human alpha activity. *Neuroimage*, **19**, 1463−1476.

Laufs, H., Krakow, K., Sterzer, P., Eger, E., Beyerle, A., Salek-Haddadi, A. & Kleinschmidt, A. (2003b) Electroencephalographic signatures of attentional and cognitive default modes in spontaneous brain activity fluctuations at rest. *Proc. Natl. Acad. Sci. USA*, **100**, 11053−11058.

Lauritzen, M. (2005) Reading vascular changes in brain imaging: Is dendritic calcium the key? *Nat. Rev. Neurosci.*, **6**, 77−85.

Lei, X., Hu, J. & Yao, D. (2012) Incorporating fMRI functional networks in EEG source imaging: A Bayesian model comparison approach. *Brain Topography*, **25**, 27−38.

Lei, X., Luo, C. & Yao, D. (2011a) Imaging epileptic networks using spatial-temporal EEG-fMRI fusion. *Int. J. Bioelectromagn.*, **13**, 249−254.

Lei, X., Ostwald, D., Hu, J., Qiu, C., Porcaro, C., Bagshaw, A.P. & Yao, D. (2011b) Multimodal functional network connectivity: An EEG-fMRI fusion in network space. *PloS One*, **6**, e24642.

Lei, X., Qiu, C., Xu, P. & Yao, D. (2010) A parallel framework for simultaneous EEG/fMRI analysis: Methodology and simulation. *Neuroimage*, **52**, 1123−1134.

Lei, X., Xu, P., Chen, A. & Yao, D. (2009a) Gaussian source model based iterative algorithm for EEG source imaging. *Comput. Biol. Med.* **39**, 978−988.

Lei, X., Xu, P., Luo, C., Zhao, J., Zhou, D. & Yao, D. (2011c) fMRI Functional Networks for EEG Source Imaging. *Hum. Brain Mapp.*, **32**, 1141−1160.

Lei, X., Yang, P. & Yao, D. (2009b) An empirical bayesian framework for brain-computer interfaces. *IEEE Trans. Neural. Syst. Rehabil. Eng.*, **17**, 521−529.

LeVan, P., Tyvaert, L., Moeller, F. & Gotman, J. (2010) Independent component analysis reveals dynamic ictal BOLD responses in EEG-fMRI data from focal epilepsy patients. *Neuroimage*, **49**, 366−378.

Litvak, V. & Friston, K. (2008) Electromagnetic source reconstruction for group studies. *Neuroimage*, **42**, 1490−1498.

Liu, A.K., Belliveau, J.W. & Dale, A.M. (1998) Spatiotemporal imaging of human brain activity using functional MRI constrained magnetoencephalography data: Monte Carlo simulations. *Proc. Natl. Acad. Sci. USA*, **95**, 8945−8950.

Liu, Z., Zhang, N., Chen, W. & He, B. (2009) Mapping the bilateral visual integration by EEG and fMRI. *Neuroimage*, **46**, 989−997.

Logothetis, N.K. (2008) What we can do and what we cannot do with fMRI. *Nature*, **453**, 869−878.

Logothetis, N.K., Pauls, J., Augath, M., Trinath, T. & Oeltermann, A. (2001) Neurophysiological investigation of the basis of the fMRI signal. *Nature*, **412**, 150−157.

Luo, C., Yao, Z., Li, Q., Lei, X., Zhou, D., Qin, Y., Xia, Y., Lai, Y., Gong, Q. & Yao, D. (2010) Imaging foci of epileptic discharges from simultaneous EEG and fMRI using the canonical HRF. *Epilepsy Res.*, **91**, 133−142.

Makeig, S., Jung, T.-P., Bell, A.J., Ghahremani, D. & Sejnowski, T.J. (1997) Blind separation of auditory event-related brain responses into independent components. *Proc. Natl. Acad. Sci. USA*, **94**, 10979−10984.

Mantini, D., Corbetta, M., Perrucci, M.G., Romani, G.L. & Del Gratta, C. (2009) Large-scale brain networks account for sustained and transient activity during target detection. *Neuroimage*, **44**, 265−274.

Mantini, D., Perrucci, M.G., Del Gratta, C., Romani, G.L. & Corbetta, M. (2007) Electrophysiological signatures of resting state networks in the human brain. *Proc. Natl. Acad. Sci. USA*, **104**, 13170−13175.

Marrelec, G. & Benali, H. (2001) Non-parametric Bayesian deconvolution of fMRI hemodynamic response function using smoothing prior. *Neuroimage*, **13**, 194−194.

Martinez-Montes, E., Valdes-Sosa, P.A., Miwakeichi, F., Goldman, R.I. & Cohen, M.S. (2004) Concurrent EEG/fMRI analysis by multiway Partial Least Squares. *Neuroimage*, **22**, 1023−1034.

Masterton, R.A.J., Harvey, A.S., Archer, J.S., Lillywhite, L.M., Abbott, D.F., Scheffer, I. E. and Jackson, G.D. (2010) Focal epileptiform spikes do not show a canonical BOLD response in patients with benign rolandic epilepsy (BECTS). *Neuroimage*, **51**, 252−260.

Mattout, J., Henson, R.N. & Friston, K.J. (2007) Canonical source reconstruction for MEG. *Comput. Intell. Neurosci.* 67613.

McKeown, M.J., Makeig, S., Brown, G.G., Jung, T.P., Kindermann, S.S., Bell, A.J. & Sejnowski, T.J. (1998) Analysis of fMRI data by blind separation into independent spatial components. *Hum. Brain Mapp.*, **6**, 160−188.

Megevand, P., Quairiaux, C., Lascano, A.M., Kiss, J.Z. & Michel, C.M. (2008) A mouse model for studying large-scale neuronal networks using EEG mapping techniques. *Neuroimage*, **42**, 591−602.

Miezin, F.M., Maccotta, L., Ollinger, J.M., Petersen, S.E. & Buckner, R.L. (2000) Characterizing the hemodynamic response: Effects of presentation rate, sampling procedure, and the possibility of ordering brain activity based on relative timing. *Neuroimage*, **11**, 735−759.

Moosmann, M., Eichele, T., Nordby, H., Hugdahl, K. & Calhoun, V.D. (2008) Joint independent component analysis for simultaneous EEG-fMRI: Principle and simulation. *Int. J. Psychophysiol.*, **67**, 212−221.

Musso, F., Brinkmeyer, J., Mobascher, A., Warbrick, T. & Winterer, G. (2010) Spontaneous brain activity and EEG microstates. A novel EEG/fMRI analysis approach to explore resting-state networks. *Neuroimage*, **52**, 1149−1161.

Niedermeyer, E. & Da Silva, F. (2010) *Electroencephalography: Basic Principles, Clinical Applications, and Related Fields*. Lippincott Williams & Wilkins.

Nunez, P. (1995) *Neocortical Dynamics and Human EEG Rhythms*. Oxford University Press, Oxford.

Nunez, P.L. & Silberstein, R.B. (2000) On the relationship of synaptic activity to macroscopic measurements: Does co-registration of EEG with fMRI make sense? *Brain Topogr*, **13**, 79−96.

Patel, A.B., de Graaf, R.A., Mason, G.F., Kanamatsu, T., Rothman, D.L., Shulman, R.G. & Behar, K.L., (2004) Glutamatergic neurotransmission and neuronal glucose oxidation are coupled during intense neuronal activation. *J. Cereb. Blood Flow Metab*, **24**, 972−985.

Phillips, C., Mattout, J., Rugg, M.D., Maquet, P. & Friston, K.J. (2005) An empirical Bayesian solution to the source reconstruction problem in EEG. *Neuroimage*, **24**, 997−1011.

Phillips, C., Rugg, M.D. & Fristont, K.J. (2002) Systematic regularization of linear inverse solutions of the EEG source localization problem. *Neuroimage*, **17**, 287−301.

Porcaro, C., Zappasodi, F., Rossini, P.M. & Tecchio, F. (2009) Choice of multivariate autoregressive model order affecting real network functional connectivity estimate. *Clin. Neurophysiol.* **120**, 436−448.

Poznanski, R.R. & Riera, J.J. (2006) fMRI models of dendritic and astrocytic networks. *J. Integr. Neurosci.*, **5**, 273−326.

Qin, Y., Xu, P. & Yao, D. (2010) A comparative study of different references for EEG default mode network: The use of the infinity reference. *Clin. Neurophysiol.*, **121**, 1981−1991.

Quiros, A., Diez, R.M. & Wilson, S.P. (2010) Bayesian spatiotemporal model of fMRI data using transfer functions. *Neuroimage*, **49**, 442−456.

Riera, J., Aubert, E., Iwata, K., Kawashima, R., Wan, X. & Ozaki, T. (2005) Fusing EEG and fMRI based on a bottom-up model: Inferring activation and effective connectivity in neural masses. *Philos. Trans. R. Soc. Lond B Biol. Sci.*, **360**, 1025−1041.

Riera, J.J. & Sumiyoshi, A. (2010) Brain oscillations: Ideal scenery to understand the neurovascular coupling. *Curr. Opin. Neurol.*, **23**, 374−381.

Rosa, M.J., Kilner, J., Blankenburg, F., Josephs, O. & Penny, W. (2010) Estimating the transfer function from neuronal activity to BOLD using simultaneous EEG-fMRI. *Neuroimage*, **49**, 1496−1509.

Sajda, P., Philiastides, M.G. & Parra, L.C. (2009) Single-trial analysis of neuroimaging data: Inferring neural networks underlying perceptual decision-making in the human brain. *IEEE Rev. Biomed. Eng.*, **2**, 97−109.

Salek-Haddadi, A., Lemieux, L., Merschhemke, M., Friston, K.J., Duncan, J.S. & Fish, D.R. (2003) Functional magnetic resonance imaging of human absence seizures. *Ann. Neurol.*, **53**, 663−667.

Sato, J.R., Rondinoni, C., Sturzbecher, M., de Araujo, D.B. & Amaro, E., Jr. (2010) From EEG to BOLD: Brain mapping and estimating transfer functions in simultaneous EEG-fMRI acquisitions. *Neuroimage*, **50**, 1416−1426.

Scheeringa, R., Bastiaansen, M.C., Petersson, K.M., Oostenveld, R., Norris, D.G. & Hagoort, P. (2008) Frontal theta EEG activity correlates negatively with the default mode network in resting state. *Int. J. Psychophysiol*, **67**, 242−251.

Scheeringa, R., Fries, P., Petersson K.-M., Oostenveld, R., Grothe, I., Norris, D.G., Hagoort, P. & Bastiaansen, M.C.M. (2011) Neuronal dynamics underlying high- and low-frequency EEG oscillations contribute independently to the human BOLD signal. *Neuron*, **69**, 572−583.

Stancak, A., Polacek, H., Vrana, J., Rachmanova, R., Hoechstetter, K., Tintra, J. & Scherg, M. (2005) EEG source analysis and fMRI reveal two electrical sources in the frontoparietal operculum during subepidermal finger stimulation. *Neuroimage*, **25**, 8−20.

Stevens, M.C., Pearlson, G.D. & Calhoun, V.D. (2009) Changes in the interaction of resting-state neural networks from adolescence to adulthood. *Hum. Brain Mapp.*, **30**, 2356−2366.

Sturzbecher, M.J., Tedeschi, W., Cabella, B.C., Baffa, O., Neves, U.P. & de Araujo D.B. (2009) Non-extensive entropy and the extraction of BOLD spatial information in event-related functional MRI. *Phys. Med. Biol.*, **54**, 161−174.

Sui, J., Adali, T., Pearlson, G., Yang, H., Sponheim, S.R., White, T. & Calhoun, V.D. (2010) A CCA + ICA based model for multi-task brain imaging data fusion and its application to schizophrenia. *Neuroimage*, **51**, 123−134.

Sui, J., Adali, T., Pearlson, G.D., Clark, V.P. & Calhoun, V.D. (2009) A method for accurate group difference detection by constraining the mixing coefficients in an ICA framework. *Hum. Brain Mapp.*, **30**, 2953−2970.

Talairach, J. & Tournoux, P. (1988) *Co-Planar Stereotaxic Atlas of the Human Brain: 3-Dimensional Proportional System: An Approach to Cerebral Imaging.* Thieme, Germany Stuttgart. p. 122.

Tao, J.X., Ray, A., Hawes-Ebersole, S. & Ebersole, J.S. (2005) Intracranial EEG substrates of scalp EEG interictal spikes. *Epilepsia*, **46**, 669−676.

Trujillo-Barreto, N., Martinez-Montes, E., Melie-Garcia, L. & Valdes-Sosa, P. (2001) A symmetrical Bayesian model for fMRI and EEG/MEG neuroimage fusion. *Int. J. Bioelectromag.*, **3**, 1.

Tyvaert, L., LeVan, P., Dubeau, F. & Gotman, J. (2009) Noninvasive dynamic imaging of seizures in epileptic patients. *Hum. Brain Mapp.*, **30**, 3993−4011.

Valdes-Sosa, P.A., Sanchez-Bornot, J.M., Sotero, R.C., Iturria-Medina, Y., Aleman-Gomez Y., Bosch-Bayard, J., Carbonell, F. & Ozaki, T. (2009a) Model driven EEG/fMRI fusion of brain oscillations. *Hum. Brain Mapp.*, **30**, 2701−2721.

Valdes-Sosa, P.A., Vega-Hernandez, M., Sanchez-Bornot, J.M., Martinez-Montes, E. & Bobes, M.A. (2009b) EEG source imaging with spatio-temporal tomographic nonnegative independent component analysis. *Hum. Brain Mapp.*, **30**, 1898−1910.

Van De Ville, D., Britz, J. & Michel, C.M. (2010) EEG microstate sequences in healthy humans at rest reveal scale-free dynamics. *Proc. Natl. Acad. Sci.* USA, **107**, 18179−18184.

Vulliemoz, S., Lemieux, L., Daunizeau, J., Michel, C.M. & Duncan, J.S. (2010a) The combination of EEG Source Imaging and EEG-correlated functional MRI to map epileptic networks. *Epilepsia*, **51**, 491−505.

Vulliemoz, S., Rodionov, R., Carmichael, D.W., Thornton, R., Guye, M., Lhatoo, S.D., Michel, C.M., Duncan, J.S. & Lemieux, L. (2010b) Continuous EEG source imaging enhances analysis of EEG-fMRI in focal epilepsy. *Neuroimage*, **49**, 3219−3229.

Wipf, D. & Nagarajan, S. (2009) A unified Bayesian framework for MEG/EEG source imaging. *Neuroimage*, **44**, 947−966.

Yao, D. (1996) The equivalent source technique and cortical imaging. *Electroencephalogr. Clin. Neurophysiol.*, **98**, 478−483.

Yao, D. (2000) Electric potential produced by a dipole in a homogeneous conducting sphere. *IEEE Trans. Biomed. Eng.*, **47**, 964−966.

Yao, D. (2001) A method to standardize a reference of scalp EEG recordings to a point at infinity. *Physiol. Meas.*, **22**, 693−711.

Yao, D., Yin, Z., Tang, X., Arendt-Nielsen, L. & Chen, A.C. (2004) High-resolution electroencephalogram (EEG) mapping: Scalp charge layer. *Phys. Med. Biol.*, **49**, 5073−5086.